Three-Dimensional Tracking of Carbon Nanotubes within Living Cells

Nigel F. Reuel,[†] Aurélie Dupont,[‡] Olivier Thouvenin,[‡] Don C. Lamb,[‡,§,*] and Michael S. Strano[†,*]

[†]Department of Chemical Engineering, Massachusetts Institute of Technology, Cambridge, Massachusetts 02139, United States, [‡]Department of Chemistry, Center for NanoScience (CeNS) and Center for Integrated Protein Science, Munich (CIPSM), Ludwig-Maximilians-Universität München, Butenandtstrasse 5-13, D-81377 München, Germany, and [§]Department of Physics, University of Illinois at Urbana—Champaign, Urbana, Illinois 61801, United States

ABSTRACT

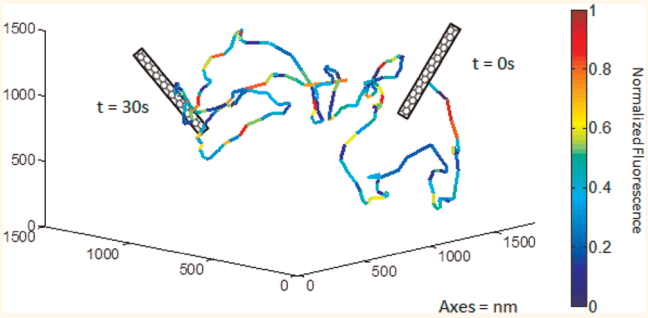

Three-dimensional tracking of single-walled carbon nanotubes (SWNT) with an orbital tracking microscope is demonstrated. We determine the viscosity regime (above 250 cP) at which the rotational diffusion coefficient can be used for length estimation. We also demonstrate SWNT tracking within live HeLa cells and use these findings to spatially map corral volumes (0.27—1.32 μm^3), determine an active transport velocity (455 nm/s), and calculate local viscosities (54—179 cP) within the cell. With respect to the future use of SWNTs as sensors in living cells, we conclude that the sensor must change the fluorescence signal by at least 4—13% to allow separation of the sensor signal from fluctuations due to rotation of the SWNT when measuring with a time resolution of 32 ms.

KEYWORDS: single-walled carbon nanotubes · three-dimensional single particle tracking · orbital tracking microscope · sensors · nIR fluorescence

Semiconducting single-walled carbon nanotubes (SWNTs), which fluoresce in the near-infrared (nIR) due to their unique band gap structure,[1] can be engineered into biosensor constructs by noncovalent wrappings that are (1) selective to target analytes (such as glucose,[2,3] NO,[4] proteins,[5] and glycans[6]) and (2) modulate the SWNT fluorescent signal when a binding event occurs.[7] However, much remains to be understood regarding SWNT interaction with biological cells and tissues, such as their mechanisms of endocytosis and trafficking, aggregation, and exocytosis.[8] Our past work utilized two-dimensional tracking of SWNTs using nIR fluorescent microscopy to elucidate the mechanistic steps of endo- and exocytosis in NIH3T3 cells.[9] Subsequently, we derived and validated a model that described the size-dependent uptake of SWNTs *via* endocytosis.[10] However, 2D tracking was limited in the spatial and temporal resolution as the particles drifted in the *z*-direction out of the focal volume or out of the field of view in the *x*—*y* direction. Feedback-based, three-dimensional nanoparticle tracking can overcome these limitations by changing the field of view or focal volume depth in real time to follow the motion of the particle. This allows one to follow SWNTs in the focus of the microscope over longer periods of time and one has the possibility to extract additional information such as corral volumes (rather than corral surfaces or regions found in 2D tracking) or determine the local viscosity experienced by the nanoparticles. As the SWNT remains in the focus of the tracking microscope, the fluorescence intensity can also be used during the trajectory to provide orientation information of anisotropic SWNT particles. Understanding the rotational behavior and corresponding signal fluctuations at varying viscosities is necessary to utilize the fluorescence intensity as a readout of the SWNT sensor.[11] Thus, not only is the pathway of the particle mapped through the cell but also the production or consumption of a specific analyte (protein, sugar, or small molecule) can be measured at different locations within a cell.

Here, we demonstrate 3D tracking of single SWNTs with an orbital tracking microscope,[12—14] and extend this technique to SWNTs localized within living HeLa cells. Mathematical modeling and analysis of the experimental *in vitro* trajectories show the effect of solution viscosity on SWNT rotational motion and confirm the hypothesis that SWNT rotation causes signal fluctuations.[15] At high viscosities (250—1000 cP), the rotation is slow enough to use the

* Address correspondence to d.lamb@lmu.de, strano@mit.edu.

Received for review March 23, 2012 and accepted May 24, 2012.

Published online May 24, 2012
10.1021/nn301298e

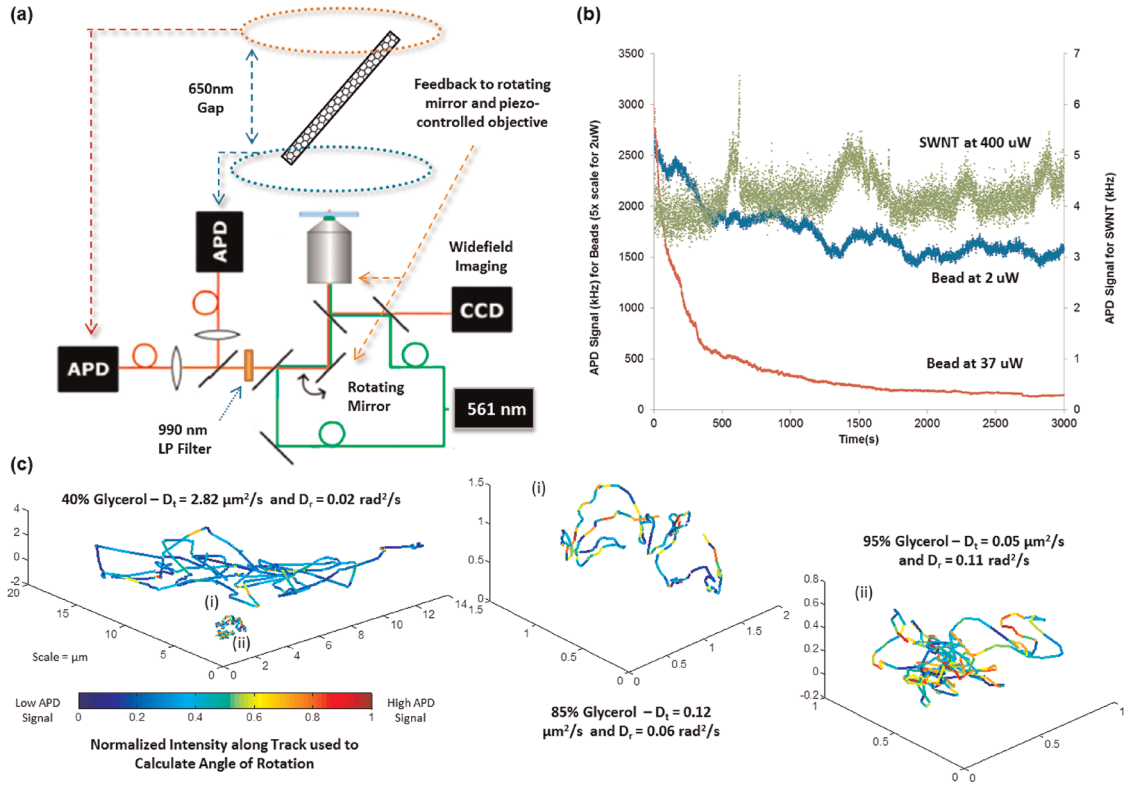

Figure 1. Three dimensional tracking of SWNTs. (a) Schematic diagram of the orbital tracking microscope with a 990 nm long-pass filter placed in the fluorescence beam path. (b) Fluorescence intensity of a SWNT and fluorescent beads for comparison at varying laser power (quantum efficiency of silicon detectors at 990 nm is less than 10%, thus, the SWNT signal is comparatively low but photostable). (c) Representative SWNT tracks at approximately 40, 85, and 95 vol % glycerol (19.3, 6.9, and 8.9 s tracks, respectively) with accompanying translational (2.82, 0.12, 0.05 $\mu m^2/s$, respectively) and rotational diffusion coefficients (0.03, 0.06, and 0.11 rad^2/s, respectively). The color of the track denotes the signal intensity to show the fluctuations during observed tracking (normalized scale).

rotational diffusion coefficient for accurate SWNT length calculations[15−18] whereas, at lower viscosities, the translational coefficient is preferred. After quantifying the translational and rotational characteristics of SWNTs as a function of viscosity, we used them to probe the viscosity of a HeLa cell. The internalized SWNTs demonstrated normal diffusion, active transport, and confined diffusion. The 3D motion of the SWNTs was used to calculate the active transport velocities and corral volumes; the relationship between SWNT rotation and translation determined *in vitro* was used to predict local apparent viscosities and SWNT lengths. Finally, we show how the rotational diffusion constant can be used to evaluate the level of background noise of a SWNT sensor and what level of quenching or fluorescence enhancement would be necessary for a statistically significant binding event to be distinguished from fluorescence fluctuations due to rotation.

RESULTS AND DISCUSSION

An orbital tracking system (with established spatial resolutions of 7−15 nm and temporal resolution of 32 ms)[12] was used to visualize chitosan wrapped SWNTs.[6] The orbital microscope utilizes an orbiting excitation beam and a real-time feedback control system (Figure 1a) to keep the particle in focus: (1) deviations from the orbit's center give rise to an intensity modulation from which the particle's position can be inferred and the orbit location is adjusted to follow the particle *via* a piezo-mirror; (2) deviations in the *z*-plane are detected *via* the difference in photon counts between the two, off-focus detection planes, and the microscope responds by a piezo-controlled objective. The microscope was originally designed for use with visible fluorescent probes[12,13] and was therefore modified for nIR detection by exchanging the emission filter with a 950 nm long-pass filter in the emission path to the silicon avalanche photo diodes (APD) (Figure 1a). The APDs have a low quantum efficiency in the nIR, but the sensitivity is still sufficient for single particle tracking. The (6,5) SWNT chirality was targeted as its excitation resonance matched the 561 nm laser source and its emission (990 nm)[1] could be detected on the APD. The large Stokes shift of the SWNT fluorescence is advantageous for tracking in live cells as the absorption of the nIR emission from the SWNTs is low ("tissue transparent window") and there will be minimal background autofluorescence.[19] Our ability to detect and track SWNTs with orbital tracking was tested using immobilized particles in cured polymer, which were first located and then tracked

while being moved in known test patterns by a piezo stage. It was found that the stock solution of SWNTs (15 mg/L) must be diluted to 0.5 vol % to detect and track individual particles. Three-dimensional single particle tracking was then performed on SWNTs in solution using the Globals for Images (SimFCS) software.[20] SWNTs exhibited their characteristic high photostability even at maximum laser power during tracking, whereas the fluorescent beads used for calibration quickly bleached at a rate dependent on laser power (Figure 1b).

As observed also in previous 2D tracking work,[15] SWNT diffusion in pure water is too rapid to allow single particle tracking in aqueous solution with our orbital tracking microscope with 32 ms per orbit (on average 500 nm in each direction per 32 ms orbit, Supporting Information, section 1). Hence, we increased the viscosity with glycerol and measured the free diffusion of SWNTs in seven different concentrations of glycerol (approximately 40, 50, 60, 75, 85, 95, and 99.5 vol% in water, Supporting Information, Table S1) (Figure 1c). As pipetting was only approximate and the hydroscopic properties of glycerol make the high glycerol concentrations unreliable, we experimentally determined the viscosity of the different solutions (Table S1). We used 190 nm diameter fluorescent beads as a calibration and extracted the viscosity from the diffusion coefficient determined from a mean square displacement (MSD) analysis assuming the Stokes−Einstein relationship:[21]

$$D = \frac{k_B T}{6\pi\eta r} \quad (1)$$

where D is the translational diffusion coefficient, k_B is the Boltzmann constant, T is temperature, η is viscosity of the solvent, and r is the radius of the spherical particle. During tracking, the fluorescence intensity of the SWNTs fluctuated (Figure 1b) significantly more than that of the control beads or of the SWNTs when placed in cured polymer. These fluctuations were attributed to the rotation of the SWNTs in solution as hypothesized by Tysboulski *et al.*[15] We also tested this hypothesis by simulating the effect of SWNT rotation in a random walk model and analyzing the simulation results with the same analysis protocol used for the acquired experimental tracks.

The length of the nanotube is an unknown parameter that needs to be determined, either through translational diffusion or rotational diffusion assuming that SWNT rotation causes fluctuations in the fluorescence signal. Calculating nanotube length from simulated and experimentally acquired trajectories and intensity data is straightforward. For translation diffusion, MSD plots (μm^2 *vs* Δt, Figure 2a insert) are created from the 3D trajectories recorded by the orbital tracking microscope, and the diffusion coefficient is determined from the slope of MSD curve[22] (code in Supporting Information, section 8). For determination of rotational diffusion, the intensity values were first scaled to geometrical angles of rotation (ranging from 0 to $^{\pi}/_{2}$) by assuming a maximum signal when the nanotube's length is parallel to the linear polarization of the impinging excitation (perpendicular to direction of the light, angle of 0) and a minimum when the nanotube is perpendicular to the polarization ($^{\pi}/_{2}$),[23] with a $\cos^2(\theta)$ dependency between these two end points.[23,24] For this assumption to hold, the nanotube must always be centered in the excitation pathway, which is a good approximation as the orbital tracking microscope continually recenters the excitation beam around the particle. This simple approximation also ignores the decrease in linear polarization of the excitation beam due to dichroics or the use of high numerical aperture objectives. However, although the approximation is simple, the comparison of calculated lengths to the measured and known physical lengths is very good. After this scaling is made, the MSD of the angle (rad^2 *vs* Δt, Figure 2a insert) is calculated and the rotational diffusion coefficients are determined from the slope of the MSD curve[22] (code in Supporting Information, section 8). The rotational diffusion of nanorods can also be determined using fluorescence correlation spectroscopy from fluctuations induced by rotation of the SWNT in a polarized excitation beam.[24] In fact, orbital tracking should allow direct observation of the rotational diffusion in FCS without being affected by translation diffusion as the excitation beam is tracking the SWNTs. However, the trajectories measured in this work were too short to perform a quantitative correlation analysis. Thus, we continued with our angle scaling approximation to find the rotational diffusion constant and used the equations outlined by Marshall *et al.*[22] without corrections for sidewall interactions to calculate the nanotube's length. This was done for both the translational (eq 2) and rotational (eq 3) diffusion coefficients (code in Supporting Information, section 8:

$$D_{trans} = \frac{k_B T\left[3\ln\left(\frac{L}{d}\right) + 2B + C\right]}{8\pi\eta L} \quad (2)$$

$$D_{rot} = \frac{k_B T 3\left[\ln\left(\frac{L}{d}\right) + A\right]}{\pi\eta L^3} \quad (3)$$

where D_{trans} and D_{rot} are the translational and rotational diffusion coefficients respectively, k_B is the Boltzmann constant, T is temperature, η is viscosity, L is the length of the nanotube, and d is the diameter of the nanotube (held constant at 0.8 nm). The parameters A, B, and C are geometrical correction factors, which for an infinitely long cylinder are −0.447, −0.114, and 0.886, respectively.[25]

The rotational diffusion coefficient is preferred to calculate SWNT length due to its higher sensitivity

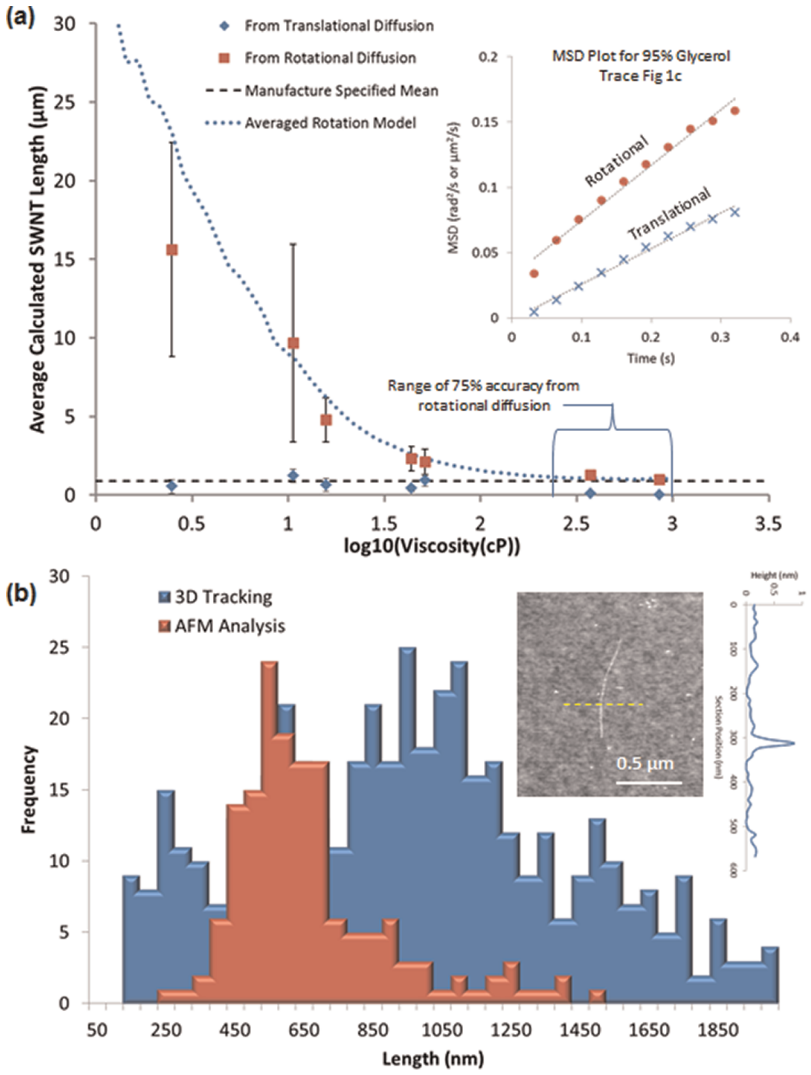

Figure 2. Measured length distribution. (a) Effect of viscosity on length predictions from rotational diffusion (red) and translational diffusion (blue). An averaged rotation model is overlaid (···) as well as the manufacture specified length of 900 nm (---). Brackets denote the range of viscosities from the random walk model where the rotational diffusion coefficient yields length calculations within 25% of the true length. The insert shows typical MSD plots used to calculate the SWNT length. (b) Histogram of SWNT lengths calculated from 3D tracking (blue) and AFM surface measurements (red). A representative AFM scan is shown in the insert along with a height profile of the single 0.8 nm diameter SWNT deposited on silicon.

(function of L^3 and not L, eq 2 and eq 3). However, this is only possible at viscosities where the rotation is slow enough for the orbit to accurately map changes in rotation between each orbit, and thus depends on the viscosity, size, orbital speed, etc. To determine at what viscosity the length calculation accuracy from rotational diffusion begins to break down for the current 32 ms minimum orbit time, a random walk model was created in Matlab (Supporting Information, section 7). A 900 nm long nanotube was simulated to take 10 000 steps at 1 ms per step dictated by translational and rotational diffusion coefficients. One thousand traces were generated for each of the 50 viscosities (ranging from 1 to 1000 cP). The "experimental traces" were simulated by averaging the positions and rotational signals of the particle for every 32 ms period. The resulting "experimental traces" were then analyzed to determine the diffusion coefficients (from MSD plots) and the coefficients were then used with eq 2 and eq 3 to determine the limits of length calculation from rotational diffusion. It was found that above 250 cP the length predictions are within 25% of the true length value when the rotational coefficient is used. At viscosities below this point, the rotational diffusion should not be used and the translational diffusion coefficient should be taken for length predictions.

This viscosity limitation is seen in our experimental data when we plot both length predictions *versus* viscosity (Figure 2a). When the model is plotted on the experimental data (dotted line Figure 2a) we see a good correspondence further establishing the assumption that we can correlate signal fluctuations to SWNT rotation. When we create a distribution of lengths (Figure 2b) calculated from the tracks (using

translational diffusion coefficients for the 40, 50, 60, 75, and 85 glycerol vol % samples and rotational for the 95 and 99.5 vol %), we find that, of the 515 successful SWNT tracks, 476 had length predictions within the expected range of 0.5 to 2 μm provided by the manufacturer. The remaining lengths (2−8 μm) were assigned to larger aggregates of SWNT and excluded from further analysis. Interestingly, the length distribution found by single particle tracking more closely fits the manufacturer's range and mode (400−2000 and 900 nm, respectively) than measurements with the same SWNT solution on a surface *via* AFM (Figure 2b). It is known that surfaces that irreversibly absorb particles will disproportionately display the smaller end of the distribution, as the smaller species diffuse the fastest to the surface from bulk and capture the available area before larger particles can reach the surface.[26−28] The experimental tracks also exhibit less accurate length predictions from translational diffusion at higher viscosities (Figure 2a). As the SWNT slows down in a more viscous solution, integrated errors begin to dominate over the microscopic movements. These errors can come from tracking inaccuracies (7−10 nm in each direction), changes in the location of the fluorescence along the length of the ∼900 nm SWNT, or errors associated with microscope drift. All of these movements cause an overestimate of the actual diffusion coefficient, particularly at high viscosity. Averaging multiple orbit steps during postprocessing to lengthen the SWNT movement between time steps improved the results but was still not sufficient to overcome the macroscopic errors (Supporting Information, section 3). To calculate accurate translational diffusion coefficients at such high viscosities, the measurement has to be optimized with great care given to the stability of the system with respect to the diffusing step sizes.

We then demonstrated 3D tracking of SWNTs in living HeLa cells and used the above relations found *in vitro* to determine local environment conditions of the cell such as apparent viscosity and regions of SWNT confinement *versus* active transport. The microscope setup (Figure 1a) allows for both tracking and widefield imaging; thus the acquired 3D traces can be mapped into a three-dimensional image of the cell volume during post processing (code available in Supporting Information, section 10). Of the 50 traces we acquired during cell experiments, 17 tracks were found to reside within a single HeLa cell and an additional track was observed in the vicinity of the exterior cell surface (Figure 3a, the other tracks were found outside cell walls). The track lengths (3.2−14.4 s) were shorter and more difficult to obtain than *in vitro* (3.2 to 90 s) due to a decreased signal-to-noise ratio within the cell. By analyzing the MSD plots of these tracks (Figure 3d and Supporting Information, section 4), we could deduce the type of diffusion (normal, convective, or confined[8,12,29]) as well as the translational and rotational diffusion constants (Figure 3b and Table 1). Ten of the tracks were found to be confined and the confinement volumes were approximated with rectangular corral volumes ranging from 0.27 to 1.32 μm^3. One track (Figure 3c) demonstrated convective diffusion with an active transport velocity of 455 nm/s (422−490 for 95% confidence with a R^2 0.998, Supporting Information, section 5), slightly larger than those found by 2D tracking of quantum dots in HeLa cells.[30] This discrepancy is likely due to the added contribution of the velocity along the third dimension that is not available in 2D measurements. Our measured transport velocity falls within the range observed for dynein[31] (centripetal and centrifugal directions were 691 ± 233 and 676 ± 214 nm/s, respectively) and other kinesin motors[32] (570 ± 20 nm/s) within HeLa cells; these are the cargo-carrying proteins that march along structural microtubules. It is also at the upper end of the range of velocities measured for actin-mediated transport (200−500 nm/s).[33]

For the SWNTs undergoing random motion within the cell, we could use the translational and rotational data of the tracked SWNTs to determine both the probable SWNT length and apparent local viscosity within the cell. This was done by first fitting the random walk model to create an expression for the ratio of length calculations *versus* solution viscosity. The form of the fit function is predicted by taking the approximate ratio of eq 3 to eq 2 and inserting the inverse relationship of diffusion constants to viscosity. By neglecting the many constants and focusing on the length values, we get a function form of

$$\frac{L_R}{L_T} = A\left(\frac{\eta}{\eta_o}\right)^{-2/3} + 1 \qquad (4)$$

where L_R and L_T are the rotational and translational length calculations, η is viscosity of the solution, η_o is viscosity of water, and A is a fit coefficient. The results from the random walk simulation are well described by eq 4 (R^2 value of 0.985) with a value of 41.31 for the fit coefficient A (Supporting Information, section 6). The same code used to calculate SWNT length *in vitro* is then used with the exception that the viscosity is now treated as an unknown parameter. The program was modified to sweep through viscosities in the range of 1−300 cP and compare the ratio of the resulting length calculations (L_R/L_T) to eq 4 until the two are in agreement. In this manner, the SWNT length and local viscosities can be determined (Table 1). The calculated internal viscosities (54−179 cP) are greater than the recent simulation results of Kalwarczyk *et al.*[34] who estimated the macroscopic cytoplasmic viscosity of HeLa cells to be 44 cP based on estimated length scales inserted in their rheological model. The higher measured viscosity is likely due to the effects of cellular crowding on macromolecular transport[35] that might not be fully captured in their model. This effect is exaggerated with SWNTs which have a length dimension

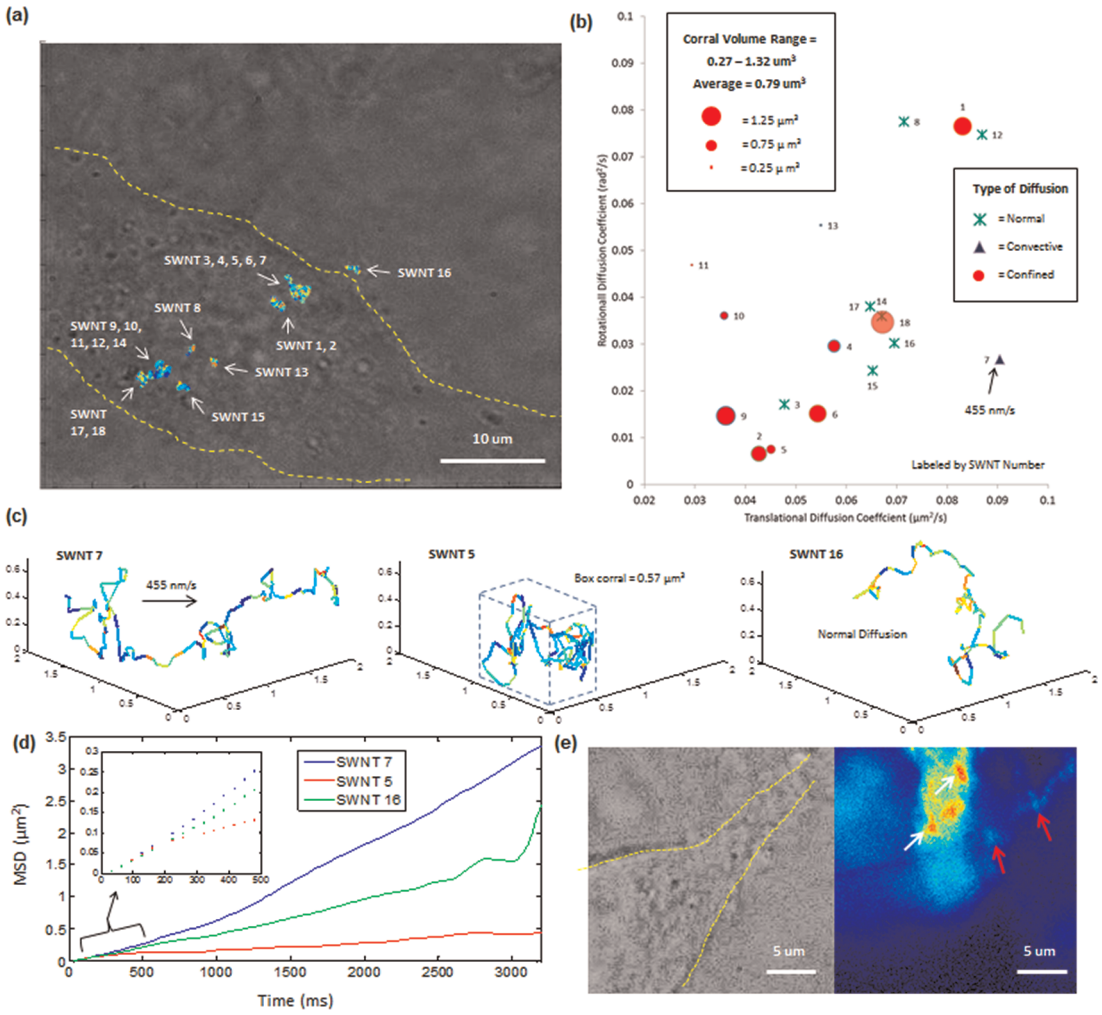

Figure 3. 3D SWNT tracks in a living HeLa cell. (a) Overlaid 2D location of 18 SWNT tracks in relation to HeLa cell (outlined in yellow). (b) Master plot of the translational, rotational diffusion coefficients, types of diffusion, and corral volumes or active transport velocities for 18 measured trajectories. Ten of the tracks demonstrated corralled diffusion with an average volume of 0.79 μm^3. (c) Representative 3D plots of three SWNT tracks demonstrating the three types of diffusion and accompanying MSD plots (d). The color of the 3D tracks denotes the level of intensity to show the fluctuations during tracking (same normalized scale as Figure 1). Internalized SWNT exhibit normal, convective, and corralled diffusion. (e) After 1.5 h, internalized SWNT have clearly formed large aggregates within (red arrows) and surrounding the cell (white arrows). Left image is from the widefield channel (yellow lines denote approximate cell boundaries) and the right is an integrated (20 s) photoluminescence image from the SWNT emission (arbitrary color scale denoting the fluorescence intensity).

2 orders of magnitude greater than large proteins. The viscosity of track 16 located near the cell membrane (71 cP) indicates that this track is indeed interacting with the cell surface and not freely diffusing in the media. This would be expected as diffusion of SWNTs in pure water was too fast to image with our current setup. Full endosomal aggregation of SWNTs occurred roughly 1.5 h after the stock solution of SWNTs was added to the cell medium (2.5% vol SWNT). Several SWNTs formed large fluorescent aggregates within the cell (Figure 3e), similar to agglomerates in endosomes observed previously by our laboratory[9,10] and others.[36−38]

With the ultimate goal of utilizing the SWNTs as internal sensors, we estimate the quality of SWNT sensors that will need to be engineered to clearly distinguish fast binding events from rotational diffusion (occurring on the time scale of the orbit or faster). From the measured radial diffusion coefficient, we calculated the average rotation during our 32 ms orbit (Table 1). By evaluating the ratio of this rotation amount to the full range of motion ($\pi/2$), we can estimate the amount of "noise" that will be present in a given track. Using a common sensor heuristic that the signal event must be three times that of the background noise, we can estimate the signal size that would be necessary to report a clear binding event, represented as a percentage of the fluorescence range presented upon SWNT rotation or $I_{max}-I_{min}$ (Table 1). For the 18 tracks, we see that the binding event would need to quench or increase the nanotube fluorescent range by 4 to 13%. This requirement can be lessened by increasing the orbital speed where fluorescence fluctuations due to rotation of the SWNT are diminished. For example, if the orbit is decreased to 3.2 ms, the fluorescence changed required for sensor applications

TABLE 1. Calculated Results from the 3D SWNT Tracks in HeLa Cell

SWNT no.	local viscosity (cP)	probable SWNT length (nm)	D_T ($\mu m^2/s$)	D_R (rad^2/s)	diffusion type	corral volume (μm^3)	convective velocity (nm/s)	avg rot during 32 ms (rad)	% ($I_{max}-I_{min}$) for significant event signal
1	78	513	0.083	0.077	confined	1.07		0.070	13%
2	72	1204	0.043	0.007	confined	0.94		0.020	4%
3	85	880	0.048	0.017	normal			0.033	6%
4	83	725	0.058	0.030	confined	0.80		0.043	8%
5	72	1147	0.045	0.008	confined	0.57		0.022	4%
6	73	899	0.054	0.015	confined	1.02		0.031	6%
7	54	706	0.090	0.027	active transport		455	0.041	8%
8	89	521	0.071	0.078	normal			0.070	13%
9	105	947	0.036	0.015	confined	1.12		0.031	6%
10	137	704	0.036	0.036	confined	0.52		0.048	9%
11	179	650	0.029	0.047	confined	0.27		0.055	10%
12	74	514	0.087	0.075	normal			0.069	13%
13	104	594	0.055	0.055	confined	0.27		0.060	11%
14	77	668	0.067	0.036	normal			0.048	9%
15	71	758	0.065	0.024	normal			0.039	8%
16	71	705	0.069	0.030	normal			0.044	8%
17	80	660	0.065	0.038	normal			0.049	9%
18	76	675	0.067	0.035	confined	1.32		0.047	9%

would be 1 to 4% and only a change of 1% would be necessary for a 0.32 ms orbit, provided the signal from the SWNT is sufficient for such quick orbits.

CONCLUSION

Herein we have successfully demonstrated 3D tracking of fluorescent SWNTs for the first time, *in vitro* and in live HeLa cells, with over 500 tracks collected from our modified orbital tracking microscope. We have created a random walk model to describe the effect of viscosity on the length calculation accuracy due to averaging during a 32 ms orbit of the excitation beam. Our model shows that, for viscosities from 250 to 1000 cP, the rotational diffusion coefficient is accurate (within 25%), but at low viscosities the translation diffusion coefficient should be used. Our *in vitro* experimental results corroborate the model by plotting the calculated lengths from both translational and rotational diffusion coefficients for the 476 experimental tracks *versus* solution viscosity. Furthermore, the excellent correspondence justifies the assumption made that fluctuations in the SWNT intensity during tracking are due to SWNT rotation as previously hypothesized.[15] AFM was also used to characterize the distribution of SWNT lengths. The length distribution was shorter than the distribution determined from 3D tracking, consistent with the property of absorbing surfaces to be covered preferentially with the smaller, faster diffusing particles.

Tracking was then demonstrated in living HeLa cells revealing normal and confined diffusion as well as active transport. By fitting to a random walk model, we created an expression that allowed us to calculate local viscosity conditions within the cell as well as the SWNT length. The intracellular tracks also demonstrated that moderately large response SWNT sensors (4 to 13% of $I_{max}-I_{min}$) are needed to overcome the signal noise introduced by rotation. This constraint is relaxed significantly when faster orbital times can be used. Although the demonstrated tracks are short (2−90 s), the photostability of the SWNTs allow for collection of longer trajectories in an orbital tracking microscope specifically designed for nIR emission (800−1600 nm). An example is an instrument with nIR sensitive detectors with, for example, Germanium or InGaAs elements. SWNT emission can also be improved with a more powerful excitation source (200 mW−1 W). With improvements in detection, one could better track the location of an individual SWNT sensor from cell internalization to eventual aggregation and also better deconvolve the fluctuating SWNT signal with a faster orbital time. In this study, we have established the contribution of SWNT rotation to signal fluctuation and its dependence on solution viscosity. This will be applied in future studies where the SWNT is utilized as an *in vivo* sensor to monitor binding events along the tracked pathway, such as reversible quenching in the presence of nitrous oxide.[39]

METHODS

Preparation of Chitosan-Wrapped SWNT Suspension. The SWNT were prepared as previously published.[6] Briefly, 3 mg of SWNT (Southwest Nanotechnologies, (6,5) chirality >70%) were added to a chitosan solution. The chitosan was made soluble by protonation in an acidic solution (add 1 vol % acetic acid).

The resulting mixture was sonicated for 40 min at 10 W amplitude with a probe tip sonicator (Cole Parmer, model CV18). The black suspension was centrifuged at 16000*g* for 2 h using a table top centrifuge (Labnet Inc.) and the supernatant was collected. The centrifugation process was repeated two more times to eliminate any SWNT aggregates. The supernatant can be stored at room temperature in a sealed container for more than 3 months without any aggregation. The final concentration of our SWNT sample was 15 mg/L as found by optical absorbance at 990 nm using the calibration value for (6,5) SWNTs of 13 mg/L for an absorption of 1 OD at 990 nm.[40]

Tracking of SWNT Particles. First, the optimal concentration of SWNTs must be determined for single particle tracking. This was done by immobilizing SWNTs in a moisture curable resin (MY-133MC from MY Polymers Ltd.) at varying SWNT concentrations and imaging the sample to see whether single particles were resolvable (Figure 1b). At concentrations greater than 0.5% vol, the sample emitted large photon counts above 950 nm, but single particles could not be detected (bright background). At a concentration of 0.5% vol, we were able to visualize single SWNTs as fluorescent diffraction-limited spots and "track" them by moving the stage holding the immobilized SWNTs in a set 2D sinusoidal and 3D box pattern as has been discussed previously.[12] Seven 100 μL SWNT-glycerol solutions were created by adding approximately 40, 50, 60, 75, 85, 95, and 99.5 μL of glycerol to 0.5 μL of SWNT stock. Particle-filtered (Millipore) pure water was added to make up the remaining volume. The solutions were bath-sonicated for 15 min in a warm bath ($T \approx 30$ °C) to ensure complete mixing of the viscous solutions and then allowed to cool to room temperature.

After calibrating the system (to determine pixel size and ensure tracking accuracy), SWNT tracking in 3D was accomplished by entrapping the SWNTs in a sample chamber and acquiring tracks using the Globals for Images (SimFCS) software from the Gratton group.[20] Sample chambers were constructed from thin (No. 1) coverslips separated by 300 μm of Parafilm (two film layers) on both sides of a small channel between the two coverslips. The SWNT solutions were drawn into the chambers *via* capillary flow and the input and output of the chamber were sealed by adding melted paraffin at the ends of the channel. The small sample chambers allowed the SWNT to freely diffuse in all 3 dimensions without wall interactions and preserved the sample for multiple days of imaging. The chambers were placed on the water-immersed objective (Nikon water immersion objective, NA 1.20 63x) and the middle of the fluid chamber was determined by observing the reflected excitation beam at the surface of the top and bottom coverslip and positioning the objective between these points. The 561 nm laser (50 mW Cobolt Jive) was set to full power (0.4 mW at the sample) to observe the SWNT. The photon counts fluctuated during a tracking event but on average were three times greater than the background count. This signal-to-noise ratio could be drastically improved by utilizing nIR detectors.

Data analysis was then done with custom Matlab programs (all available in Supporting Information, sections 7−10). The text log output from the SimFCS software was parsed to extract the *X*, *Y*, and *Z* coordinates as well as the photon counts from the upper and lower detectors. As the traces contained some dead time before and after the real tracking events or jumping between different tracked particles, another automated program was used to analyze the data and find significant tracking events (code in Supporting Information, section 8). Specified criteria were longer tracks (greater than 100 steps) that had small internal step lengths (total squared displacement less than 3×10^4 nm^2 between steps or average of 100 nm in each direction). Finally, another program was used to analyze each of these significant traces with the following steps: (1) calculate MSD plots from the position and rotational data, (2) fit the first 10% of the time steps in the MSD plot to determine the translational and rotational diffusion coefficients, and (3) calculate lengths using the equations detailed by Marshall *et al.*[22] A distribution of the lengths was then created from the individual measurements.

Tracking of SWNT Particles in Live HeLa Cells. Live HeLa cells were seeded at a density of 1×10^4 cells/well into eight well chamber slides (IBIDI). The cell culture media was replaced prior to experiment by warm DPBS buffer, and the sample was maintained at 37 °C on the microscope stage. A target cell was visualized using the widefield channel of the microscope. First, the center of the cell was approximated by bringing the intracellular compartments in sharp focus and then a stack of five images below and five above the center point were acquired at a step resolution of 200 nm using an external *z*-axis control. This stack of images was later used to reconstruct the cell volume (*via* the darker cell walls) and see if the overlaid SWNT tracks were within the cell volume. SWNTs were added from the stock solution to the media (10 μL, final concentration 2.5% vol) without disturbing the cell in focus. The SWNTs diffuse too quickly in aqueous solution to be tracked with the current setup. After 30 min, the SWNTs are taken up by the HeLa cells and the motion of the SWNTs can then be followed. After overlaying the acquired tracks, 17 were found within the cell volume along with one extra-cellular SWNT resting on or near the plasma membrane.

AFM Imaging of SWNTs. For AFM measurements, the stock solution of chitosan SWNTs was diluted by 10× and deposited on a clean silicon wafer. After allowing for physisorption for 30 min, the chip was washed with water three times and then dried with nitrogen. The SWNTs on the chip are then imaged with AFM (Asylum Research) using a silicon nitride tip (Olympus Micro Cantilievers, resonant frequency of 70 kHz, spring constant of 2 N/m) in tapping mode at 700mW drive set point and scan angle of 90°. A scan area of 5 μm square and scan frequency of 0.5 Hz was found to visualize the SWNTs well. The SWNT lengths were measured by the multipoint length determining tool of Gwyddion software (freely available online).

Conflict of Interest: The authors declare no competing financial interest.

Acknowledgment. This work was supported by a grant from the National Science Foundation to M.S.S. N.F.R. gratefully acknowledges a DAAD Summer Research Grant and NSF Graduate Fellowship. D.C.L. gratefully acknowledges the financial support of the DFG through the SFB 646 and the Nanosystems Initative Munich (NIM) and the Ludwig-Maximilians-University Munich through the LMUInnovativ BioImaging Network (BIN).

Supporting Information Available: Sections 1−10 as described in the text. This material is available free of charge *via* the Internet at http://pubs.acs.org.

REFERENCES AND NOTES

1. Bachilo, S. M.; Strano, M. S.; Kittrell, C.; Hauge, R. H.; Smalley, R. E.; Weisman, R. B. Structure-Assigned Optical Spectra of Single-Walled Carbon Nanotubes. *Science* **2002**, *298*, 2361–2366.
2. Barone, P. W.; Strano, M. S. Reversible Control of Carbon Nanotube Aggregation for a Glucose Affinity Sensor. *Angew. Chem., Int. Ed.* **2006**, *45*, 8138–8141.
3. Barone, P. W.; Parker, R. S.; Strano, M. S. *In Vivo* Fluorescence Detection of Glucose Using a Single-Walled Carbon Nanotube Optical Sensor: Design, Fluorophore Properties, Advantages, and Disadvantages. *Anal. Chem.* **2005**, *77*, 7556–7562.
4. Zhang, J. Q.; Boghossian, A. A.; Barone, P. W.; Rwei, A.; Kim, J. H.; Lin, D. H.; Heller, D. A.; Hilmer, A. J.; Nair, N.; Reuel, N. F.; *et al.* Single Molecule Detection of Nitric Oxide Enabled by d(AT)(15) DNA Adsorbed to Near Infrared Fluorescent Single-Walled Carbon Nanotubes. *J. Am. Chem. Soc.* **2011**, *133*, 567–581.
5. Ahn, J. H.; Kim, J. H.; Reuel, N. F.; Barone, P. W.; Boghossian, A. A.; Zhang, J. Q.; Yoon, H.; Chang, A. C.; Hilmer, A. J.; Strano, M. S. Label-free, Single Protein Detection on a Near-Infrared Fluorescent Single-Walled Carbon Nanotube/Protein Microarray Fabricated by Cell-free Synthesis. *Nano Lett* **2011**, *11*, 2743–2752.
6. Reuel, N. F.; Ahn, J. H.; Kim, J. H.; Zhang, J. Q.; Boghossian, A. A.; Mahal, L. K.; Strano, M. S. Transduction of

Glycan-Lectin Binding Using Near-Infrared Fluorescent Single-Walled Carbon Nanotubes for Glycan Profiling. *J. Am. Chem. Soc.* **2011**, *133*, 17923–17933.
7. Boghossian, A. A.; Zhang, J. Q.; Barone, P. W.; Reuel, N. F.; Kim, J. H.; Heller, D. A.; Ahn, J. H.; Hilmer, A. J.; Rwei, A.; Arkalgud, J. R.; *et al*. Near-Infrared Fluorescent Sensors Based on Single-Walled Carbon Nanotubes for Life Sciences Applications. *Chemsuschem* **2011**, *4*, 848–863.
8. Strano, M. S.; Jin, H. Where is it heading? Single-Particle Tracking of Single-Walled Carbon Nanotubes. *ACS Nano* **2008**, *2*, 1749–1752.
9. Jin, H.; Heller, D. A.; Strano, M. S. Single-Particle Tracking of Endocytosis and Exocytosis of Single-Walled Carbon Nanotubes in NIH-3T3 Cells. *Nano Lett* **2008**, *8*, 1577–1585.
10. Jin, H.; Heller, D. A.; Sharma, R.; Strano, M. S. Size-Dependent Cellular Uptake and Expulsion of Single-Walled Carbon Nanotubes: Single Particle Tracking and a Generic Uptake Model for Nanoparticles. *ACS Nano* **2009**, *3*, 149–158.
11. Boghossian, A. A.; Zhang, J. Q.; Le Floch-Yin, F. T.; Ulissi, Z. W.; Bojo, P.; Han, J. H.; Kim, J. H.; Arkalgud, J. R.; Reuel, N. F.; Braatz, R. D.; *et al*. The Chemical Dynamics of Nanosensors Capable of Single-Molecule Detection. *J. Chem. Phys.* **2011**, *135*, 084124, 1–10.
12. Dupont, A.; Lamb, D. C. Nanoscale Three-Dimensional Single Particle Tracking. *Nanoscale* **2011**, *3*, 4532–4541.
13. Katayama, Y.; Burkacky, O.; Meyer, M.; Brauchle, C.; Gratton, E.; Lamb, D. C. Real-Time Nanomicroscopy *via* Three-Dimensional Single-Particle Tracking. *Chemphyschem* **2009**, *10*, 2458–2464.
14. Levi, V.; Ruan, Q.; Kis-Petikova, K.; Gratton, E. Scanning FCS, a Novel Method for Three-Dimensional Particle Tracking. *Biochem. Soc. Trans.* **2003**, *31*, 997–1000.
15. Tsyboulski, D. A.; Bachilo, S. M.; Kolomeisky, A. B.; Weisman, R. B. Translational and Rotational Dynamics of Individual Single-Walled Carbon Nanotubes in Aqueous Suspension. *ACS Nano* **2008**, *2*, 1770–1776.
16. Duggal, R.; Pasquali, M. Dynamics of Individual Single-Walled Carbon Nanotubes in Water by Real-Time Visualization. *Phys. Rev. Lett.* **2006**, *96*, 246104, 1–4.
17. Boghossian, A. A.; Choi, J. H.; Ham, M. H.; Strano, M. S. Dynamic and Reversible Self-Assembly of Photoelectrochemical Complexes Based on Lipid Bilayer Disks, Photosynthetic Reaction Centers, and Single-Walled Carbon Nanotubes. *Langmuir* **2011**, *27*, 1599–1609.
18. Branca, C.; Magazu, V.; Mangione, A. Determination of MWNTs Length-to-Diameter Ratio by Static and Dynamic Light Scattering. *Diam. Relat. Mater.* **2005**, *14*, 846–849.
19. Yi, H.; Ghosh, D.; Ham, M.-H.; Qi, J.; Barone, P. W.; Strano, M. S.; Belcher, A. M. M13 Phage-Functionalized Single-Walled Carbon Nanotubes as Nanoprobes for Second Near-Infrared Window Fluorescence Imaging of Targeted Tumors. *Nano Lett.* **2012**, *12*, 1176–1183.
20. Gratton, E. Globals Software for Spectroscopy and Images. http://www.lfd.uci.edu/globals/ (accessed 12.9.11).
21. Edward, J. T. Molecular Volumes and Stokes–Einstein Equation. *J. Chem. Educ.* **1970**, *47*, 261–270.
22. Marshall, B. D.; Davis, V. A.; Lee, D. C.; Korgel, B. A. Rotational and Translational Diffusivities of Germanium Nanowires. *Rheol. Acta* **2009**, *48*, 589–596.
23. Duesberg, G. S.; Loa, I.; Burghard, M.; Syassen, K.; Roth, S. Polarized Raman Spectroscopy on Isolated Single-Wall Carbon Nanotubes. *Phys. Rev. Lett.* **2000**, *85*, 5436–5439.
24. Tsay, J. M.; Doose, S.; Weiss, S. Rotational and Translational Diffusion of Peptide-Coated CdSe/CdS/ZnS Nanorods Studied by Fluorescence Correlation Spectroscopy. *J. Am. Chem. Soc.* **2006**, *128*, 1639–1647.
25. Broersma, S. Viscous Force and Torque Constants for a Cylinder. *J. Chem. Phys.* **1981**, *74*, 6989–6990.
26. Anancharungsuk, W.; Taweepreda, W.; Wirasate, S.; Thonggoom, R.; Tangboriboonrat, P. Reduction of Surface Friction of Natural Rubber Film Coated with PMMA Particle: Effect of Particle Size. *J. Appl. Polym. Sci.* **2010**, *115*, 3680–3686.
27. Qiu, H. W.; Lee, W. Y.; Sukhishvili, S. A. Layer-by-Layer Self-Assembly of Ceramic Particles for Coating Complex Shape Substrates. *J. Am. Ceram. Soc.* **2006**, *89*, 1180–1187.
28. Rogers, S. S.; Venema, P.; Sagis, L. M. C.; van der Linden, E.; Donald, A. M. Measuring the Length Distribution of a Fibril System: A Flow Birefringence Technique Applied to Amyloid Fibrils. *Macromolecules* **2005**, *38*, 2948–2958.
29. Bickel, T. A Note on Confined Diffusion. *Phys. A* **2007**, *377*, 24–32.
30. Jiang, X. E.; Rocker, C.; Hafner, M.; Brandholt, S.; Dorlich, R. M.; Nienhaus, G. U. Endo- and Exocytosis of Zwitterionic Quantum Dot Nanoparticles by Live HeLa Cells. *ACS Nano* **2010**, *4*, 6787–6797.
31. Kobayashi, T.; Murayama, T. Cell Cycle-Dependent Microtubule-Based Dynamic Transport of Cytoplasmic Dynein in Mammalian Cells. *PLoS One* **2009**, *4*, e7827.
32. Courty, S.; Luccardini, C.; Bellaiche, Y.; Cappello, G.; Dahan, M. Tracking Individual Kinesin Motors in Living Cells Using Single Quantum-Dot Imaging. *Nano Lett.* **2006**, *6*, 1491–1495.
33. Pierobon, P.; Achouri, S.; Courty, S.; Dunn, A. R.; Spudich, J. A.; Dahan, M.; Cappello, G. Velocity, Processivity, and Individual Steps of Single Myosin V Molecules in Live Cells. *Biophys. J.* **2009**, *96*, 4268–4275.
34. Kalwarczyk, T.; Ziebacz, N.; Bielejewska, A.; Zaboklicka, E.; Koynov, K.; Szymanski, J.; Wilk, A.; Patkowski, A.; Gapinski, J.; Butt, H. J.; *et al*. Comparative Analysis of Viscosity of Complex Liquids and Cytoplasm of Mammalian Cells at the Nanoscale. *Nano Lett* **2011**, *11*, 2157–2163.
35. Ando, T.; Skolnick, J. Crowding and Hydrodynamic Interactions Likely Dominate *in Vivo* Macromolecular Motion. *Proc. Natl. Acad. Sci. U.S.A.* **2010**, *107*, 18457–18462.
36. Porter, A. E.; Gass, M.; Bendall, J. S.; Muller, K.; Goode, A.; Skepper, J. N.; Midgley, P. A.; Welland, M. Uptake of Noncytotoxic Acid-Treated Single-Walled Carbon Nanotubes into the Cytoplasm of Human Macrophage Cells. *ACS Nano* **2009**, *3*, 1485–1492.
37. Yehia, H.; Draper, R.; Mikoryak, C.; Walker, E.; Bajaj, P.; Musselman, I.; Daigrepont, M.; Dieckmann, G.; Pantano, P. Single-Walled Carbon Nanotube Interactions with HeLa Cells. *J. Nanobiotechnol.* **2007**, *5*, 1–17.
38. Cui, H. F.; Vashist, S. K.; Al-Rubeaan, K.; Luong, J. H. T.; Sheu, F. S. Interfacing Carbon Nanotubes with Living Mammalian Cells and Cytotoxicity Issues. *Chem. Res. Toxicol.* **2010**, *23*, 1131–1147.
39. Kim, J. H.; Heller, D. A.; Jin, H.; Barone, P. W.; Song, C.; Zhang, J.; Trudel, L. J.; Wogan, G. N.; Tannenbaum, S. R.; Strano, M. S. The Rational Design of Nitric Oxide Selectivity in Single-Walled Carbon Nanotube Near-Infrared Fluorescence Sensors for Biological Detection. *Nat. Chem.* **2009**, *1*, 473–481.
40. Ming, Z.; Diner, B. A. Solution Redox Chemistry of Carbon Nanotubes. *J. Am. Chem. Soc.* **2004**, *126*, 15490–15494.